Article

Ultrafast Excited-State Dynamics of Nanoscale Near-Infrared Emissive Polymersomes

Timothy V. Duncan, P. Peter Ghoroghchian, Igor V. Rubtsov, Daniel A. Hammer, and Michael J. Therien

J. Am. Chem. Soc., **2008**, 130 (30), 9773-9784 • DOI: 10.1021/ja711497w • Publication Date (Web): 09 July 2008

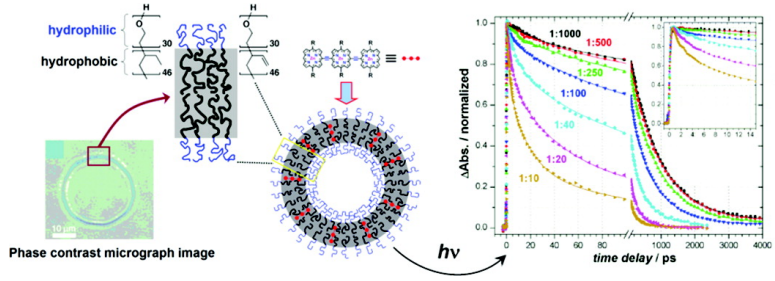

More About This Article

Additional resources and features associated with this article are available within the HTML version:

- Supporting Information
- Access to high resolution figures
- Links to articles and content related to this article
- Copyright permission to reproduce figures and/or text from this article

View the Full Text HTML

J|A|C|S
ARTICLES

Published on Web 07/09/2008

Ultrafast Excited-State Dynamics of Nanoscale Near-Infrared Emissive Polymersomes

Timothy V. Duncan,[†] P. Peter Ghoroghchian,[†,‡] Igor V. Rubtsov,[†,§] Daniel A. Hammer,[‡] and Michael J. Therien*[,||]

Department of Chemistry, University of Pennsylvania, Philadelphia, Pennsylvania 19104, School of Engineering and Applied Science, and Institute for Medicine and Engineering, University of Pennsylvania, Philadelphia, Pennsylvania 19104, and Department of Chemistry, Duke University, Durham, North Carolina 27708

Received January 13, 2008; E-mail: michael.therien@duke.edu

Abstract: Formed through cooperative self-assembly of amphiphilic diblock copolymers and electronically conjugated porphyrinic near-infrared (NIR) fluorophores (NIRFs), NIR-emissive polymersomes (50 nm to 50 μm diameter polymer vesicles) define a family of organic-based, soft-matter structures that are ideally suited for deep-tissue optical imaging and sensitive diagnostic applications. Here, we describe magic angle and polarized pump−probe spectroscopic experiments that: (i) probe polymersome structure and NIRF organization and (ii) connect emitter structural properties and NIRF loading with vesicle emissive output at the nanoscale. Within polymersome membrane environments, long polymer chains constrain ethyne-bridged oligo(porphinato)zinc(II) based supermolecular fluorophore (**PZn$_n$**) conformeric populations and disperse these **PZn$_n$** species within the hydrophobic bilayer. Ultrafast excited-state transient absorption and anisotropy dynamical studies of NIR-emissive polymersomes, in which the **PZn$_n$** fluorophore loading per nanoscale vesicle is varied between 0.1−10 mol %, enable the exploration of concentration-dependent mechanisms for nonradiative excited-state decay. These experiments correlate fluorophore structure with its gross spatial arrangement within specific nanodomains of these nanoparticles and reveal how compartmentalization of fluorophores within reduced effective dispersion volumes impacts bulk photophysical properties. As these factors play key roles in determining the energy transfer dynamics between dispersed fluorophores, this work underscores that strategies that modulate fluorophore and polymer structure to optimize dispersion volume in bilayered nanoscale vesicular environments will further enhance the emissive properties of these sensitive nanoscale probes.

Introduction

The design of biocompatible, near-infrared (NIR) emissive, high-emission-dipole-strength nanoscale agents defines an important materials chemistry challenge and an area of considerable biomedical interest.[1,2] To date, many investigators have focused on the development of quantum dots (inorganic semiconductor nanocrystals) for both *in vitro* and *in vivo* fluorescence-based imaging.[3–12] Although quantum dots often exhibit superior optical characteristics relative to traditional organic fluorophores, they may ultimately achieve limited clinical utility, as their constituent materials are inherently toxic.[13–19] As such, the design of alternative, organic-based fluorescent nanoparticles is an area of active investigation that aims to generate novel agents that possess large magnitude irradiance, high photostability, and yet are also biocompatible.[20–37] Many of these systems, including several com-

[†] Department of Chemistry, University of Pennsylvania.
[‡] Institute for Medicine and Engineering, University of Pennsylvania.
[§] Present address: Department of Chemistry, Tulane University, Louisiana 70118.
[||] Department of Chemistry, Duke University, Durham, NC 27708.

(1) Sevick-Muraca, E. M.; Houston, J. P.; Gurfinkel, M. *Curr. Opin. Chem. Biol.* **2002**, *6*, 642–650.
(2) Frangioni, J. V. *Curr. Opin. Chem. Bio.* **2003**, *7*, 626–634.
(3) Chan, W. C. W.; Nie, S. *Science* **1998**, *281*, 2016–2018.
(4) Bruchez, M.; Moronne, M.; Gin, P.; Weiss, S.; Alivisatos, A. P. *Science* **1998**, *281*, 2013–2016.
(5) Wu, X.; Liu, H.; Liu, J.; Haley, K. N.; Treadway, J. A.; Larson, J. P.; Ge, N.; Peale, F.; Bruchez, M. P. *Nat. Biotechnol.* **2003**, *21*, 41–46.
(6) Jaiswal, J. K.; Mattoussi, H.; Mauro, J. M.; Simon, S. M. *Nat. Biotechnol.* **2003**, *21*, 47–51.
(7) Alivisatos, P. *Nat. Biotechnol.* **2004**, *22*, 47–52.
(8) Gao, X.; Cui, Y.; Levenson, R. M.; Chung, L. W. K.; Nie, S. *Nat. Biotechnol.* **2004**, *22*, 969–976.
(9) Medintz, I. L.; Uyeda, H. T.; Goldman, E. R.; Mattoussi, H. *Nat. Mat.* **2005**, *4*, 435–446.
(10) Michalet, X.; Pinaud, F. F.; Bentolila, L. A.; Tsay, J. M.; Doose, S.; Li, J. J.; Sundaresan, G.; Wu, A. M.; Gambhir, S. S.; Weiss, S. *Science* **2005**, *307*, 538–544.
(11) Jaiswal, J. K.; Simon, S. M. *Trends Cell Biol.* **2004**, *14*, 497–504.
(12) Kim, S.; Lim, Y. T.; Soltesz, E. G.; De Grand, A. M.; Lee, J.; Nakayama, A.; Parker, J. A.; Mihaljevic, T.; Laurence, R. G.; Dor, D. M.; Cohn, L. H.; Bawendi, M. G.; Frangioni, J. V. *Nat. Biotechnol.* **2004**, *22*, 93–97.
(13) Hoshino, A.; Fujioka, K.; Oku, T.; Suga, M.; Sasaki, Y. F.; Ohta, T.; Yasuhara, M.; Suzuki, K.; Yamamoto, K. *Nano Lett.* **2004**, *4*, 2163–2169.
(14) Shiohara, A.; Hoshino, A.; Hanaki, K.; Suzuki, K.; Yamamoto, K. *Microbiol. Immunol.* **2004**, *48*, 669–675.
(15) Derfus, A. M.; Chan, W. C. W.; Bhatia, S. N. *Nano Lett.* **2004**, *4*, 11–18.
(16) Oberdörster, G.; Oberdörster, E.; Oberdörster, J. *Env. Health Persp.* **2005**, *113*, 823–839.
(17) Lovric, J.; Bazzi, H. S.; Cuie, Y.; Fortin, G. R. A.; Winnik, F. M.; Maysinger, D. *J. Mol. Med.* **2005**, *83*, 377–385.

mercially available emissive probes, feature large numbers of conventional organic fluorophores dispersed within a polymer-based nanoparticle host; despite numerous emissive probe platforms that exploit this approach, there have been relatively few studies that rigorously explore the range of factors that influence the emissive capacity of such organic-based fluorophore-nanoparticle systems. There is thus not only a continuing need to delineate new soft matter emissive nanoparticle archetypes having enhanced photophysical properties but also a substantial motivation to identify factors that control the emissive output of such soft-matter structures.

Meso-to-*meso* ethyne-bridged oligo(porphinato)zinc(II)-based supermolecules (**PZn$_n$** compounds) define a family of near-infrared fluorophores (NIRFs) that exhibit substantial molar absorptivities throughout the visible and NIR regions,[38–42] large NIR quantum yields,[42] high photobleaching thresholds (>500 mW/cm^2 under continuous illumination for >20 min),[43] and no chemical or photobased *in vitro* toxicity.[44] Through cooperative self-assembly with amphiphilic diblock copolymers, these π-conjugated multi-[(porphinato)zinc] NIRFs can be dispersed, noncovalently, at high concentrations (10 mol/wt%) within the thick synthetic membranes of polymersomes (50 nm to 50 μm diameter polymer vesicles) (Scheme 1).[45–47] These NIR-emissive polymersomes define a family of organic-based, soft matter nano-to-mesoscale structures ideally suited for *in vivo* optical imaging and sensitive diagnostic applications.[43] Previous studies have focused, for example, upon delineation of a rich photophysical diversity[48] and quantification of fluorophore membrane-loading[49] in these emissive assemblies; notably, membrane incorporation of a wide range of related multiporphyrinic fluorophores has enabled precise emission energy modulation over a broad domain of the visible and near-infrared spectrum (600−900 nm).[43,48] These studies underscore that controlling polymer-to-fluorophore intermembranous physicochemical interactions at the nanoscale finely tunes the bulk photophysical properties of these soft, macromolecular, optical materials.[48,50] In this report, we explore the excited-state dynamics of NIR-emissive polymersomes and probe the factors that modulate the observed photophysics of **PZn$_n$** fluorophores in nanoscale, synthetic bilayered vesicular environments.

An extensive body of experimental[51–64] and theoretical[51,63,65–70] literature describes the photophysical properties of membrane-dispersed fluorophores; much of this work has interrogated energy transfer reactions and fluorescence quenching pathways that derive from excitation migration to dark trap aggregates. Building on this work, we examine herein the visible and NIR ultrafast transient absorption dynamics of NIR-emissive polymersomes, utilizing a combination of excited-state anisotropy and magic-angle pump−probe measurements to correlate how fluorophore structure influences the nature of dispersion and the extent of excited-state interchromophoric electronic coupling within the bilayered vesicular environment. We interrogate three highly conjugated *meso*-to-*meso* ethyne-bridged tris[(porphinato)zinc(II)] species (**3,5-peg-PZn$_3$**, **3,5-alk-PZn$_3$**, and **2,6-peg-PZn$_3$**), which differ only in the nature of their respective

(18) Kirchner, C.; Liedl, T.; Kudera, S.; Pellegrino, T.; Javier, A. M.; Gaub, H. E.; Stölzle, S.; Fertig, N.; Parak, W. J. *Nano Lett.* **2005**, *5*, 331–338.
(19) Hardman, R. *Env. Health Persp.* **2006**, *114*, 165–172.
(20) Graf, C.; Schärtl, W.; Fischer, K.; Hugenberg, N.; Schmidt, M. *Langmuir* **1999**, *15*, 6170–6180.
(21) Kolodny, L. A.; Willard, D. M.; Carillo, L. L.; Nelson, M. W.; van Orden, A. *Anal. Chem.* **2001**, *73*, 1959–1966.
(22) Fu, H.-B.; Yao, J.-N. *J. Am. Chem. Soc.* **2001**, *123*, 1434–1439.
(23) An, B.-K.; Kwon, S.-K.; Jung, S.-D.; Park, S. Y. *J. Am. Chem. Soc.* **2002**, *124*, 14410–14415.
(24) Yang, C.-S.; Chang, C.-H.; Tsai, P.-J.; Chen, W.-Y.; Tseng, F.-G.; Lo, L.-W. *Anal. Chem.* **2004**, *76*, 4465–4471.
(25) Schiro, P. G.; Kwok, A. S. *Optics Express* **2004**, *12*, 2857–2863.
(26) Nayak, S.; Lyon, L. A. *Angew. Chem., Int. Ed.* **2005**, *44*, 7686–7708.
(27) Chinnayelka, S.; McShane, M. J. *Anal. Chem.* **2005**, *77*, 5501–5511.
(28) Han, M.; Hara, M. *J. Am. Chem. Soc.* **2005**, *127*, 10951–10955.
(29) Wang, F.; Han, M.-Y.; Mya, K. Y.; Wang, Y.; Lai, Y.-H. *J. Am. Chem. Soc.* **2005**, *127*, 10350–10355.
(30) Makarava, N.; Parfenov, A.; Baskakov, I. V. *Biophys. J.* **2005**, *89*, 572–580.
(31) Sun, Y.-Y.; Liao, J.-H.; Fang, J.-M.; Chou, P.-T.; Shen, C.-H.; Hsu, C.-W.; Chen, L.-C. *Org. Lett.* **2006**, *8*, 3713–3716.
(32) Zhao, L.; Lei, Z.; Li, X.; Li, S.; Xu, J.; Peng, B.; Huang, W. *Chem. Phys. Lett.* **2006**, *420*, 480–483.
(33) Wu, C.; Szymanski, C.; McNeill, J. *Langmuir* **2006**, *22*, 2956–2960.
(34) Zhu, L.; Wu, W.; Zhu, M.-Q.; Han, J. J.; Hurst, J. K.; Li, A. D. Q. *J. Am. Chem. Soc.* **2007**, *129*, 3524.
(35) Hou, X.; Liu, B.; Deng, X.; Zhang, B.; Chen, H.; Luo, R. *Anal. Biochem.* **2007**, *368*, 100–110.
(36) Rounds, R. M.; Ibey, B. L.; Beier, H. T.; Pishko, M. V.; Coté, G. L. *J. Fluorescence* **2007**, *17*, 57–63.
(37) Watanabe, R.; Munemasa, T.; Matsumura, M.; Fujimaki, M. *Meth. Find. Exp. Clin. Pharm.* **2007**, *29*, 321–327.
(38) Lin, V. S.-Y.; DiMagno, S. G.; Therien, M. J. *Science* **1994**, *264*, 1105–1111.
(39) Lin, V. S.-Y.; Therien, M. J. *Chem.−Eur. J.* **1995**, *1*, 645–651.
(40) Angiolillo, P. J.; Lin, V. S.-Y.; Vanderkooi, J. M.; Therien, M. J. *J. Am. Chem. Soc.* **1995**, *117*, 12514–12527.
(41) Susumu, K.; Therien, M. J. *J. Am. Chem. Soc.* **2002**, *124*, 8550–8552.
(42) Duncan, T. V.; Susumu, K.; Sinks, L. E.; Therien, M. J. *J. Am. Chem. Soc.* **2006**, *128*, 9000–9001.
(43) Ghoroghchian, P. P.; Frail, P. R.; Susumu, K.; Blessington, D.; Brannan, A. K.; Bates, F. S.; Chance, B.; Hammer, D. A.; Therien, M. J. *Proc. Nat. Acad. Sci. U.S.A.* **2005**, *102*, 2922–2927.
(44) Wu, S. P.; Lee, I.; Ghoroghchian, P. P.; Frail, P. R.; Zheng, G.; Glickson, J. D.; Therien, M. J. *Bioconj. Chem.* **2005**, *16*, 542–550.
(45) Discher, B. M.; Bermudez, H.; Hammer, D. A.; Discher, D. E.; Won, Y.-Y.; Bates, F. S. *J. Phys. Chem. B* **2002**, *106*, 2848–2854.
(46) Discher, D. E.; Eisenberg, A. *Science* **2002**, *297*, 967–973.
(47) Antonietti, M.; Förster, S. *Adv. Mater.* **2003**, *15*, 1323–1333.
(48) Ghoroghchian, P. P.; Frail, P. R.; Susumu, K.; Park, T.-H.; Wu, S.; Uyeda, H. T.; Hammer, D. A.; Therien, M. J. *J. Am. Chem. Soc.* **2005**, *127*, 15388–15390.
(49) Ghoroghchian, P. P.; Lin, J. J.; Brannan, A. K.; Bates, F. S.; Frail, P. R.; Therien, M. J.; Hammer, D. A. *Soft Matter* **2006**, *2*, 1–9.
(50) Ghoroghchian, P. P.; Frail, P. R.; Li, G.; Zupancich, J. A.; Bates, F. S.; Hammer, D. A.; Therien, M. J. *Chem. Mater.* **2007**, *19*, 1309–1318.
(51) Stryer, L. *Annu. Rev. Biochem.* **1978**, *47*, 819–846.
(52) Lakowicz, J. R.; Prendergast, F. G.; Hogen, D. *Biochemistry* **1979**, *18*, 508–519.
(53) Hoekstra, D. *Biochemistry* **1982**, *21*, 2833.
(54) Arvinte, T.; Cudd, A.; Hildenbrand, K. *Biochim. Biophys. Acta* **1986**, *860*, 215.
(55) Johansson, L. B.-Å.; Niemi, A. *J. Phys. Chem.* **1987**, *91*, 3020–3023.
(56) MacDonald, R. *J. Biol. Chem.* **1990**, *265*, 13533–13539.
(57) Yamazaki, I.; Tamai, N.; Yamazaki, T. *J. Phys. Chem.* **1990**, *94*, 516–525.
(58) Caruso, F.; Grieser, F.; Murhpy, A.; Thistlethwaite, P.; Urquhart, R.; Almgren, M.; Wistus, E. *J. Am. Chem. Soc.* **1991**, *113*, 4838–4843.
(59) Brown, R. S.; Brennan, J. D.; Krull, U. J. *J. Chem. Phys.* **1994**, *100*, 6019–6027.
(60) Karolin, J.; Johansson, L. B. Å.; Strandberg, L.; Ny, T. *J. Am. Chem. Soc.* **1994**, *116*, 7801–7806.
(61) Xiao, W.; Lin, S.; Taguchi, A. K. W.; Woodbury, N. W. *Biochemistry* **1994**, *33*, 8313–8322.
(62) Matzinger, S.; Hussey, D. M.; Fayer, M. D. *J. Phys. Chem. B* **1998**, *102*, 7216–7224.
(63) Lakowicz, J. R. *Principles of Fluorescence Spectroscopy*, 3rd ed; Springer: New York, 2006.
(64) Loura, L. M. S.; Prieto, M. *J. Phys. Chem. B* **2000**, *104*, 6911–6919.
(65) Zumofen, G.; Blumen, A. *J. Chem. Phys.* **1982**, *76*, 3713–3731.
(66) Hare, F. *Biophys. J.* **1983**, *42*, 205–218.
(67) Baumann, J.; Fayer, M. D. *J. Chem. Phys.* **1986**, *85*, 4087–4107.
(68) Boulu, L. G.; Patterson, L. K.; Chauvet, J. P.; Kozak, J. J. *J. Chem. Phys.* **1987**, *86*, 503–507.
(69) Johansson, L. B. Å.; Engström, S.; Lindberg, M. *J. Chem. Phys.* **1992**, *96*, 3844–3856.
(70) Toptygin, D.; Svobodova, J.; Konopasek, I.; Brand, L. *J. Chem. Phys.* **1992**, *96*, 7919–7930.

Scheme 1. (A) Depiction of **PZn_3** Fluorophore Dispersion within PEO−PBD NIR-Emissive Polymersome Environments and (B) Hydrophobic Bilayer Thicknesses (L) of **PEO_{30}−PBD_{46}** and **PEO_{80}−PBD_{125}** Polymersomes[a]

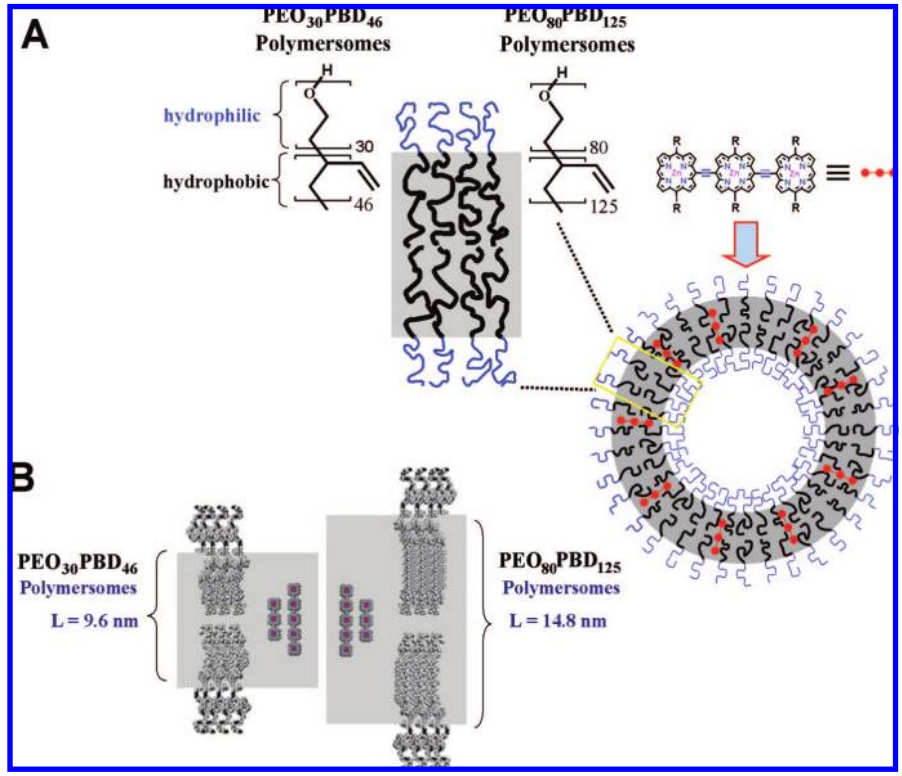

[a] Generic **PZn_3** and **PZn_5** fluorophores are also shown, to scale, for comparison.

Chart 1. Structures of Ethyne-Bridged Porphyrin Arrays **3,5-peg-PZn_3**, **3,5-alk-PZn_3**, **2,6-alk-PZn_3**, and **3,5-peg-PZn_5**

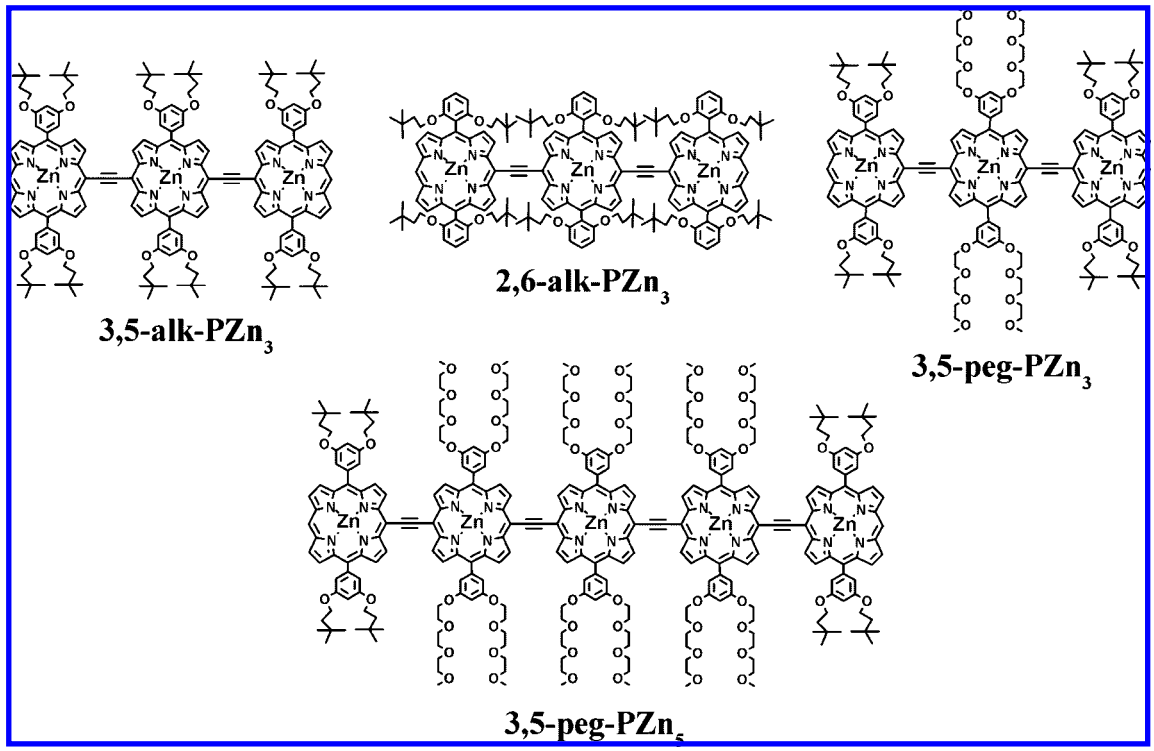

porphyrin pendant side chains, as well as a highly conjugated ethyne-bridged porphyrin pentamer (**3,5-peg-PZn_5**), in polymersomal environments; these structures are depicted in Chart 1. Two constituent amphiphilic diblock copolymers of polyethyleneoxide-b-1,2-polybutadiene, **PEO_{30}−PBD_{46}** and **PEO_{80}−PBD_{125}**, were used to form the NIR-emissive polymersome assemblies investigated herein. These polymers self-assemble to form bilayered vesicles with differing membrane hydrophobic core thicknesses (L; L(**PEO_{30}−PBD_{46}**) ∼9.6 nm; L(**PEO_{80}−PBD_{125}**) ∼14.8 nm)[71] and, hence, different volumes

for NIRF dissolution (Scheme 1). Within polymersome membrane environments, long polymer chains constrain fluorophores to individual nanodomains and control interchromophoric interactions.[48–50] In order to probe concentration-dependent mechanisms for nonradiative decay, NIR-emissive polymersomes were formed from various molar ratios of NIRF:polymer (χ = 0.001, 0.002, 0.004, 0.01, 0.025, 0.05, and 0.1), quantitatively varying membrane loading per vesicle (0.1−10 mol%).[49]

This work describes the first systematic ultrafast spectroscopic investigation of an organic-based NIR-fluorescent nanoparticle system and demonstrates key relationships between fluorophore structure, nanoparticle composition, and the excited-state dynamics. These transient optical studies provide mechanistic insights and aid in the continuing development of these organic-based fluorescent nanoparticles as ultrasensitive optical probes.

Experimental Section

Syntheses of Fluorophores. The syntheses and characterization data for all fluorophores have been reported elsewhere (see Supporting Information).[41,44,72]

Vesicle Preparation. Formation of giant (>1 μm diameter) and small (<300 nm diameter) NIR-emissive polymersomes followed procedures described elsewhere.[43] Brief descriptions of these procedures are provided in the Supporting Information.

Steady State Absorption and Emission Spectroscopy. These methods are detailed in the Supporting Information.

Pump−Probe Transient Absorption Spectroscopy. A detailed description of the instrumentation and sample preparation procedures are provided in the Supporting Information and has also been provided elsewhere.[73,74] Excited-state dynamics were probed within the Q_x manifold bleaching signature, centered at $\lambda \approx$ 804 nm for **PZn$_3$** species. Representative transient absorption spectra of membrane-dispersed **PZn$_3$** species are shown in the Supporting Information (Figure S12), along with a description of observed spectral features. In contrast to similar pump−probe experiments performed in THF solution,[42,73] the transient optical experiments involving emissive polymersomes are complicated by significant light scattering at water-polymersome interfaces. This is most problematic at low (χ < 0.01) fluorophore loadings, where signal-to-noise is minimal. Excited-state anisotropy decay was monitored by adjusting the relative polarizations of the pump and probe pulses using an achromatic half-waveplate to rotate the beam polarization. Excited-state anisotropy measurements were conducted with pump and probe polarization in parallel (0°) and perpendicular (90°) relative orientations and at the magic angle (54.7°) to follow isotropic dynamics. Probe beam polarization was controlled by a thin-film polarizer. In order to achieve high photoselection, pump fluences at the sample were kept as low as possible (<0.2 mJ/cm^2) while still allowing for reasonable absorption intensities (>10 mOD). Typical anisotropy values reported derive from data acquired over 10 scans having alternating probe beam polarization and calculated by the expression:

$$r(t) = \frac{I_{\parallel}(t) - I_{\perp}(t)}{I_{\parallel}(t) + 2I_{\perp}(t)} \quad (1)$$

Results and Discussion

A. Electronic Absorption and Emission Spectroscopy. Multimeric porphyrin compounds that feature a *meso*-to-*meso* ethyne-bridged linkage topology (**PZn$_n$** compounds) manifest low energy Q_x-state derived $\pi-\pi^*$ excited-states that are polarized exclusively along the long supermolecular axis.[38,39,41,42,75–77] The lowest energy optical transitions of these species gain in intensity and shift progressively to the red with increasing numbers of conjugated porphyrin units. These oligomeric compounds define exceptional low band gap chromophores that are notable in that they possess NIR $S_1 \rightarrow S_0$ fluorescence quantum yields which are enhanced dramatically with respect to those of their monomeric precursors, and emission bands tunable over a 700−950 nm regime.[38–42,73,75,76] In solution, structural heterogeneity at ambient temperatures is manifest and derives primarily from the low barrier to rotation about the *meso*-to-*meso* ethyne bridge, causing a torsional angle distribution between the respective macrocycle least-squares planes of **PZn$_n$** oligomers.[39,42,73,75,76] This conformational inhomogeneity is manifested in the optical spectra of these species. For example, the electronic absorption spectrum of **3,5-peg-PZn$_3$** recorded in THF solution (Figure 1A, black line) shows an *x*-polarized Q-state absorption envelope deriving from a Boltzmann-weighted distribution of **PZn$_3$** conformers that differ with respect to their respective interporphyryl torsional angles and wavelength-dependent absorption oscillators strengths.[42,73] The THF solution electronic absorption spectra of **3,5-alk-PZn$_3$** and **2,6-alk-PZn$_3$**, which bear respective 3,5-bis(3,3-dimethylbutoxy)phenyl and

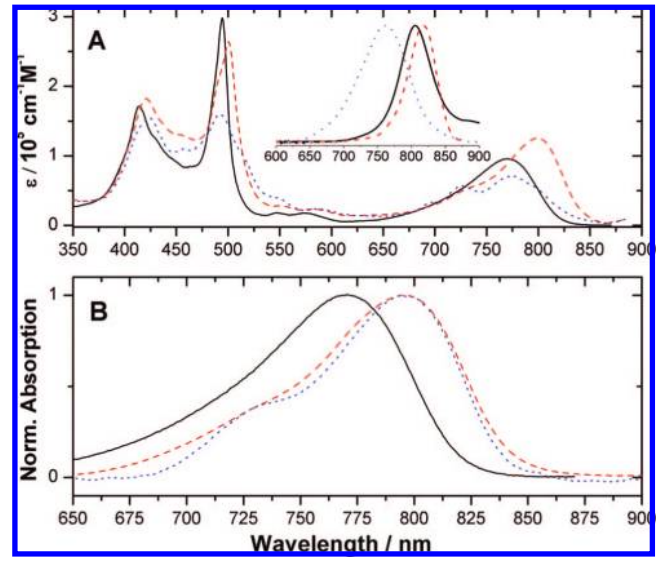

Figure 1. (A) Electronic absorption spectra of: **3,5-peg-PZn$_3$** in THF solution (solid black), **3,5-alk-PZn$_3$** dispersed at a 10% fluorophore:polymer molar ratio in **PEO$_{30}$−PBD$_{46}$** (L = 9.6 nm) polymersomes (dashed red), and **2,6-alk-PZn$_3$** dispersed at a 10% fluorophore:polymer molar ratio in **PEO$_{30}$−PBD$_{46}$** polymersomes (dotted blue). The electronic absorption spectra of **2,6-alk-PZn$_3$** and **3,5-alk-PZn$_3$** in THF solution are identical to the spectrum of **3,5-peg-PZn$_3$** in THF solution (data not shown). The inset shows the corresponding normalized emission spectra after excitation at 510 nm. (B) Normalized electronic absorption spectra in the Q_x absorption manifold of **3,5-peg-PZn$_3$** in THF solution (solid black) and within **PEO$_{30}$-PBD$_{46}$** polymersomes loaded at 10 (dashed red) and 0.2% (dotted blue) fluorophore:polymer molar ratios.

(71) Bermudez, H.; Brannan, A. K.; Hammer, D. A.; Bates, F. S.; Discher, D. E. *Macromolecules* **2002**, *35*, 8203–8208.
(72) Frail, P. R.; Susumu, K.; Huynh, M.; Fong, J.; Kikkawa, J. M.; Therien, M. J. *Chem. Mater.* **2007**, *19*, 6062–6064.
(73) Rubtsov, I. V.; Susumu, K.; Rubtsov, G. I.; Therien, M. J. *J. Am. Chem. Soc.* **2003**, *125*, 2687–2696.
(74) Duncan, T. V.; Rubtsov, I. V.; Uyeda, H. T.; Therien, M. J. *J. Am. Chem. Soc.* **2004**, *126*, 9474–9475.
(75) Kumble, R.; Palese, S.; Lin, V. S.-Y.; Therien, M. J.; Hochstrasser, R. M. *J. Am. Chem. Soc.* **1998**, *120*, 11489–11498.
(76) Shediac, R.; Gray, M. H. B.; Uyeda, H. T.; Johnson, R. C.; Hupp, J. T.; Angiolillo, P. J.; Therien, M. J. *J. Am. Chem. Soc.* **2000**, *122*, 7017–7033.
(77) Duncan, T. V.; Wu, S. P.; Therien, M. J. *J. Am. Chem. Soc.* **2006**, *128*, 10423–10435.

2,6-bis(3,3-dimethylbutoxy)phenyl substituents (Scheme 1), are virtually identical to the Figure 1A spectrum of **3,5-peg-PZn$_3$**.

Figure 1A also depicts electronic absorption spectra of **3,5-alk-PZn$_3$** (red) and **2,6-alk-PZn$_3$** (blue) dispersed at a 10% fluorophore:polymer mole ratio ($\chi = 0.1$, moles fluorophore per moles constituent polymer) in **PEO$_{30}$-PBD$_{46}$** ($L \approx 9.6$ nm) polymersomes. The spectrum of **3,5-peg-PZn$_3$** dispersed at a 10% fluorophore:polymer mole ratio in **PEO$_{30}$-PBD$_{46}$** polymersomes (data not shown) is similar to that recorded for membrane-dispersed **3,5-alk-PZn$_3$**. The Q_x-state manifold λ_{max} and full width at half-maximum (fwhm) values are tabulated in Table S1 (Supporting Information). The Figure 1A spectra demonstrate a few key points regarding the nature of fluorophore dispersion within the polymersome bilayer: (i) in nanoscale polymersomes, membrane-dispersed **3,5-alk-PZn$_3$** and **3,5-peg-PZn$_3$** manifest Q_x absorption manifold red-shifts ($\Delta\lambda_{max}$(**3,5-alk-PZn$_3$**) = 25 nm [$\sim$410 cm^{-1}]; $\Delta\lambda_{max}$(**3,5-peg-PZn$_3$**) = 28 nm [$\sim$450 cm^{-1}]) and integrated oscillator strength intensification ($\sim$20%) relative to the analogous spectrum recorded in THF solvent (black), indicating that membrane-dispersed ethyne-bridged porphyrin arrays experience a reduction in ground-state structural heterogeneity characterized by a narrower PZn−PZn torsional angle distribution centered about a diminished mean macrocycle-macrocyle torsional angle.[48,73] Consistent with this, the Q_x-state electronic absorption manifolds of membrane-dispersed **3,5-alk-PZn$_3$** and **3,5-peg-PZn$_3$** narrow significantly (fwhm(**3,5-alk-PZn$_3$**) = 1200 cm^{-1}; fwhm(**3,5-peg-PZn$_3$**) = 1265 cm^{-1}) with respect to their analogous absorption manifolds evident in THF solvent (fwhm(**3,5-alk-PZn$_3$**) = 1474 cm^{-1}; fwhm(**3,5-peg-PZn$_3$**) = 1386 cm^{-1}).

In contrast to the red-shift of the Q_x-state absorption manifolds manifested by **3,5-alk-PZn$_3$** and **3,5-peg-PZn$_3$** within emissive polymersome bilayers, polymersome-dispersed **2,6-alk-PZn$_3$** exhibits a moderate blue-shift of this absorption envelope (Figure 1A, blue line) relative to that evinced by this chromophore in THF solvent. Note that in contrast to the polymersomes that feature **3,5-alk-PZn$_3$** and **3,5-peg-PZn$_3$** emitters, the Q_x absorption manifold of **PEO$_{30}$−PBD$_{46}$** membrane-dispersed **2,6-alk-PZn$_3$** reveals several distinct transitions. These data suggest that for this **PZn$_3$** structure, steric factors make possible multiple PZn-PZn interplanar torsional angle minima in the hydrophobic bilayer. Such structural inhomogeneity derives from the bulky 2,6-alkoxyphenyl porphyrinic ancillary groups, which convert the overall chromophore geometry from a biconcave wedge to a cylinder.[48] The combination of this gross structural modification with the change in spatial distribution of the **2,6-alk-PZn$_3$** solubilizing substituents relative to those of **3,5-alk-PZn$_3$** and **3,5-peg PZn$_3$**, perturb the local arrangement of polymer chains within the polymersonal bilayer and help drive augmented aggregate formation, consistent with the broadened spectroscopic features manifested by **PEO$_{30}$−PBD$_{46}$** vesicles that disperse **2,6-alk-PZn$_3$**.

Although the nature of solvation within the polymersome matrix effects shifts in the electronic absorption bands of the **PZn$_3$** and **PZn$_5$** species (Supporting Information, Table S1) relative to that observed in THF solvent, equally significant spectroscopic changes are correlated with the extent of fluorophore loading in these vesicles. The normalized Q_x-state regions of the electronic absorption spectra of **3,5-peg-PZn$_3$** in THF solution (black), dispersed at 10 (red) and 0.2% (blue) fluorophore:polymer mole ratios in **PEO$_{30}$−PBD$_{46}$** polymersomes are shown in Figure 1B. Note that while the Q_x-state absorption manifolds of the two membrane-dispersed species have identical λ_{max} values (795 nm), the Q_x absorption envelope of the 10 mol% loaded sample (fwhm = 1265 cm^{-1}) is broadened with respect to the analogous set of transitions in the 1:500 loaded sample (fwhm = 1094 cm^{-1}), consistent with more extensive intermolecular fluorophore-fluorophore interactions. Membrane-dispersed **3,5-alk-PZn$_3$** and **3,5-peg-PZn$_5$** manifest similar spectral changes upon increased loading as indicated by their respective concentration-dependent $S_0 \rightarrow S_1$ fwhm values (Supporting Information, Table S1). In **PEO$_{30}$−PBD$_{46}$** polymersome samples where **3,5-peg-PZn$_3$** is dispersed at 10 and 0.2% fluorophore:polymer mole ratios, the Q_x-state absorption manifold spectral breadths [fwhm(10 mol %) = 1265 cm^{-1}; fwhm(0.2 mol %) = 1094 cm^{-1}] exceed that for analogous polymersome preparations that disperse **3,5-alk-PZn$_3$** (fwhm(10 mol %) = 1200 cm^{-1}; fwhm(0.2 mol %) = 1051 cm^{-1}], suggesting that for a given fluorophore:polymer mole ratio in these nanoscale vesicles, **3,5-peg-PZn$_3$** exhibits augmented intermolecular interactions relative to **3,5-alk-PZn$_3$** (*vide infra*). Although a 10% fluorophore:polymer mole ratio represents the largest chromophore loading level interrogated in our dynamical studies, it is noted that at higher fluorophore loadings, **PZn$_n$** Q_x absorption manifolds broaden and red shift extensively, indicating that the 10% fluorophore:polymer mole ratio represents the approximate limit of fluorophore solubility within a polymersome bilayer composed of **PEO$_{30}$−PBD$_{46}$** diblock copolymers.

The steady-state emission spectra of **PZn$_n$** fluorophores dispersed within **PEO$_{30}$−PBD$_{46}$** vesicles (Figure 1A, inset) exhibit emission bands which are 50 - 70% narrower (fwhm values) than their respective lowest-energy electronic absorption bands (Table S1). Note that the Stokes shift magnitude scales with the fluorophore molar loading percentage (Table S1), suggesting that polymersomes that feature progressively larger fluorophore concentrations within the bilayer manifest more complex excited-state dynamics. These simple relationships involving the extent of fluorophore loading, **PZn$_3$** absorption and emission band spectral breadths, and the magnitude of the fluorescence Stokes shift, are not apparent in the analogous spectra of polymersome membrane dispersed **2,6-alk-PZn$_3$**, as the emission bands of these species remain broad regardless of the extent of fluorophore loading percentage (Table S1), consistent with extensive conformational inhomogeneity and the substantial degree of aggregate formation manifest for this emitter when dispersed within the bilayer environment (*vide supra*). Additionally, the integrated emission intensity of **2,6-alk-PZn$_3$**:**PEO$_{30}$−PBD$_{46}$** polymersomes remains small compared to that evinced in dilute THF solution over a 0.1−10% fluorophore:polymer loading range, likely due to static quenching contributions that arise from large concentrations of chromophore aggregates. Interestingly, the emission λ_{max} (760 nm) of these nanoscale vesicles is blue-shifted with respect to the Q_x manifold lowest-energy absorption λ_{max} (775 nm), suggesting that the fraction of aggregate states that contributes to the absorption band oscillator strength as a function of wavelength increases with increasing wavelength, and features diminished emission quantum yield.

The per **PZn$_n$** molecule steady-state emission intensity evident in THF solvent remains unchanged in the polymersome matrix at low ($\chi < 0.004$) fluorophore:polymer mole ratios. However, as χ is increased beyond 0.004 (0.4% fluorophore:polymer mole ratio), the emission intensity per molecule drops as indicated in Figure S9.[48] On a per vesicle basis, emission intensity follows a different trend (Figure S10). While individual chromophores

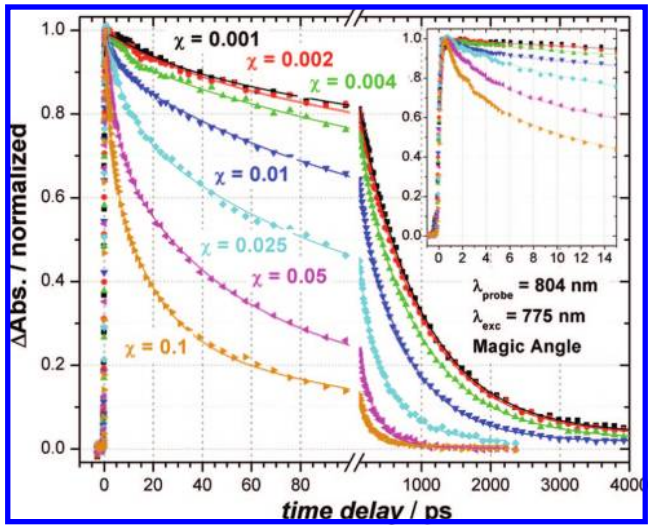

Figure 2. Normalized intensities and transient bleaching signature centered at 804 nm for **3,5-peg-PZn$_3$**, dispersed at several fluorophore:polymer loading levels in **PEO$_{30}$−PBD$_{46}$** (L = 9.6 nm) polymersomes, plotted as a function of time delay in picoseconds. Solid lines represent multiexponential fits to the data. Fitting parameters are tabulated in Table S2 (Supporting Information). (Inset) Expanded window of the 0−10 ps time domain. Experimental conditions: λ_{exc} = 775 nm, λ_{probe} = 804 nm, solvent = water, room temperature.

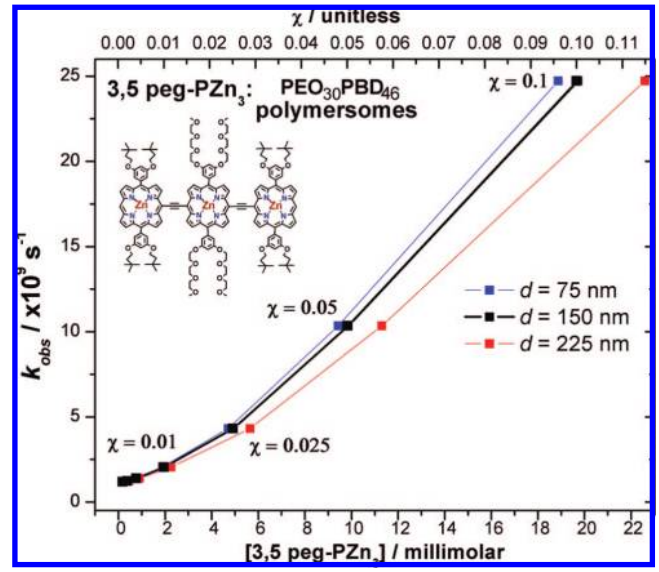

Figure 3. Rate constants for excited-state deactivation (k_{obs} values) of **3,5-peg-PZn$_3$** dispersed within **PEO$_{30}$−PBD$_{46}$** (L = 9.6 nm) polymersomes as functions of fluorophore-to-polymer mole ratio (χ, upper axis) and absolute fluorophore concentration ([**3,5-peg-PZn$_3$**], lower axis). The black squares plotted as a function of χ represent real data points; to convert these data into absolute concentration, polymersome volumes were estimated (Supporting Information). The blue and red, respectively, reflect the same data derived using the minimum (75 nm) and maximum (225 nm) values of polymersome diameters present in the sample solution, demonstrating the effective range of absolute fluorophore concentrations resulting from identical χ values.

at higher loadings have an increased probability of manifesting a diminished fluorescence quantum yield, there are also more of them; the net result is that emission intensity per vesicle initially increases as a function of χ, but then plateaus at a fluorophore:polymer mole ratio of ∼ 5%. Figure S10 also demonstrates that for a given level of fluorophore loading, vesicles containing **3,5-peg-PZn$_3$** have slightly less per vesicle integrated emission intensity than vesicles that disperse **3,5-alk-PZn$_3$**. This is consistent with electronic absorption (*vide supra*) and transient optical data (*vide infra*) that suggest that membrane-dispersed **3,5-peg-PZn$_3$** is more prone to aggregation than **3,5-alk-PZn$_3$**.

B. Excited-State Dynamics of Nanoscale NIR-Emissive Polymersomes Based on 3,5-peg-PZn$_3$ Fluorophores and PEO$_{30}$−PBD$_{46}$ Diblock Copolymers. The normalized transient absorption intensities of the **3,5-peg-PZn$_3$** bleaching signature centered at ∼800 nm as a function of time delay at several loading percentages in **PEO$_{30}$−PBD$_{46}$** (L ∼ 9.6 nm) polymersomes are plotted in Figure 2 (see the Supporting Information section for a full description of and figures depicting transient absorption spectral features). The figure demonstrates that at high **3,5-peg-PZn$_3$** fluorophore loadings of the polymersome bilayer, the excited-state lifetime (τ_{avg}) becomes short (χ = 0.1, τ < 100 ps) compared to that determined in analogous nanoscale polymersomes where the fluorophore concentration is low (χ = 0.001, τ > 800 ps). For **3,5-peg-PZn$_3$** loadings where χ < 0.004, the excited-state decay dynamics are well described by a multiexponential fit which is dominated by a single term (i.e., the associated amplitude of one exponential is >85%), reflecting the simple excited-state decay process expected for dilute fluorophore conditions; in samples where $\chi \geq 0.004$, the excited-state decay profiles are modeled by multiexponential functions in which multiple exponential terms have significant amplitude, indicating more complex excited-state dynamics in nanoscale polymersomes that feature more significant fluorophore concentrations. Averaged excited-state lifetimes (calculated by weighting the individual exponential components by their relative amplitudes), as well as associated observed excited-state deactivation rate constants, k_{obs} (τ_{avg}^{-1}), are tabulated in Table S2; as indicated in Figure 2, τ_{avg} drops precipitously at **3,5-peg-PZn$_3$** loadings exceeding a 0.4% fluorophore:polymer mole ratio. Furthermore, the Figure 2 inset shows that in the most concentrated samples (χ = 0.05 and 0.1), a significant fraction (∼30%) of the decay amplitude is dominated by a newly arising component with τ < 5 ps.

The k_{obs} values tabulated (Table S2) for **3,5-peg-PZn$_3$** dispersed in **PEO$_{30}$−PBD$_{46}$** (L ∼ 9.6 nm) polymersomes are plotted in Figure 3 as a function of mole ratio (χ, upper axis) and absolute fluorophore concentration. Dynamic light-scattering measurements reveal that vesicle diameters of the NIR-emissive polymersomes probed in these experiments range from 75 to 225 nm. Thus, a sample of fluorophore-loaded polymersomes possessing an absolute χ value manifests a distribution of fluorophore molar concentrations. The molar concentration ([**3,5-peg-PZn$_3$**]) axis depicted on the bottom of Figure 3 was calculated assuming uniform fluorophore dispersion throughout the respective vesicular bilayer volumes (see Supporting Information). The black squares represent the k_{obs} values correlated to molar concentrations calculated for a mean vesicular diameter of 150 nm. The blue and red squares represent k_{obs} values correlated for fluorophore concentrations calculated at the minimum (75 nm) and maximum (225 nm) diameters of the statistical range; the red and blue squares therefore bear no relationship to the upper axis of this figure. Although the range of emissive polymersome diameters is large (75−225 nm), the statistical distribution of **3,5-peg-PZn$_3$** molar concentrations within the polymersomal bilayer is small.

Figure 3 chronicles the relationship between NIR fluorophore concentration and the average measured excited-state lifetime of **3,5-peg-PZn$_3$** fluorophores dispersed in the polymersomal

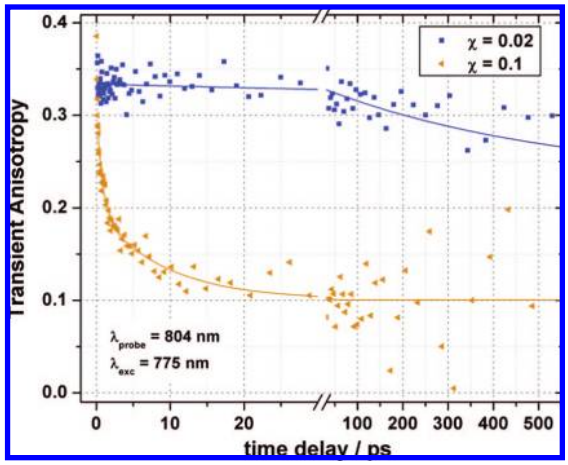

Figure 4. Excited-state anisotropy of **3,5-peg-PZn$_3$** dispersed at 0.2% (blue squares) and 10% (orange triangles) fluorophore:polymer ratios in **PEO$_{30}$−PBD$_{46}$** (L = 9.6 nm) polymersomes as a function of time delay. The solid lines represent multiexponential fits of the data. Experimental conditions: λ_{exc} = 775 nm, λ_{probe} = 804 nm, solvent = water, room temperature.

bilayer. Note that while fluorescence quenching arises typically from a combination of dynamic (collisional) and static (ground-state complex formation) quenching mechanisms, static contributions are generally not reflected in lifetime measurements,[63] so the concentration-dependent excited-state deactivation rate constants depicted in Figure 3 only represent the dynamic counterpart of the overall fluorescence quenching behavior. Consistent with experiments that probe fluorescence quenching in membrane environments,[53,55,56,59,63,67–69] it is important to underscore that significant collisional quenching contributions are incompatible with these nanoscale constructs, as these would require a high rate of fluorophore translational motion within the polymersome matrix. In this regard, the transient absorption spectra demonstrate virtually no spectral diffusion related to conformational changes on the experimental time scale (Figure S12), so molecular translational motion would be similarly inhibited.

In order to further probe the dynamic excited-state quenching mechanism in these systems, pump−probe transient anisotropy measurements were carried out as a function of **3,5-peg-PZn$_3$** fluorophore concentration in the polymersomal bilayer. Figure 4 plots the time-dependent transient anisotropy, r(t), for the singly degenerate x-polarized Q-state of **3,5-peg-PZn$_3$** dispersed in **PEO$_{30}$−PBD$_{46}$** (L ∼ 9.6 nm) polymersomes at 0.2 (χ = 0.002) and 10% (χ = 0.1) fluorophore:polymer mole ratios (λ_{ex} = 775 nm; λ_{probe} = 804 nm). The excited-state anisotropy determined in samples where χ = 0.002 shows a weak time dependence ($\tau \gg 5$ ns); this dependence contrasts that observed for **PZn$_3$** fluorophores in dilute THF solution, where excited-state anisotropies decay to zero with (rotational) depolarization correlation times (ϕ) of ∼1.25 ns (Supporting Information, Figure S1). The Figure 4 data obtained for samples that feature a 0.2% fluorophore:polymer mole ratio are consistent with a rigid environment that enforces a large barrier to **PZn$_3$** rotation.[78] Note that while the initial transient anisotropy, r_0, was 0.4 for **PZn$_3$** chromophores in THF (Supporting Information), indicating that the ground and initially prepared **PZn$_3$** excited states are mutually parallel and directed along the highly conjugated molecular axis, in the χ = 0.002 sample, $r_0 \approx 0.34$. As this experiment was repeated at several excitation fluences to ensure maximum photoselection, this sub-0.4 r_0 value likely derives from light scattering, a phenomenon established[79] to yield erroneously low anisotropy values for emitters dispersed in membranous assemblies. Note that in the χ = 0.1 sample, where light scattering is less problematic, $r_0 \approx 0.39$ (Figure 4).

In contrast to the relative invariance of the excited-state anisotropy with time delay for χ = 0.002 NIR-emissive polymersome samples, when **3,5-peg-PZn$_3$** is dispersed at a 10% fluorophore:polymer mole ratio in **PEO$_{30}$−PBD$_{46}$** polymersomes (χ = 0.1), the **3,5-peg-PZn$_3$** excited-state anisotropy is lost with a depolarization correlation time (ϕ) of 14.3 ps; here, ϕ is the weighted average of three exponential terms (orange line, Figure 4). Given that such fast quenching of the excited-state anisotropy occurs only at high (χ > 0.01) **3,5-peg-PZn$_3$** loadings (see Figure S2), these observed dynamics likely derive in large part from Förster energy migration[80,81] between closely situated fluorophores that feature a distribution of orientations. Interestingly, while the **3,5-peg-PZn$_3$** excited-state anisotropy decay in the χ = 0.1 polymersome compositions (Figure 4) is quite fast ($\phi \approx$ 14.3 ps) compared to the analogous decay in THF solution ($\phi \approx$ 1.24 ns), r(t) does not decay to zero in the membrane-dispersed sample at long time delays; instead, the excited-state anisotropy asymptotically approaches a value of ∼0.1. These data indicate that while fluorophore orientation is completely random in solution, the polymersome bilayer enforces a net **3,5-peg-PZn$_3$** alignment in the polymersome bilayer, and energy transfer processes thus do not lead to complete excited-state absorption depolarization.[82]

Average interfluorophore distances for a given fluorophore:polymer mole ratio (χ) can be roughly estimated by assuming a spherical shape for **PZn$_3$** fluorophores (diameter = 3.0 nm) and homogeneous dispersion throughout the entire hydrophobic bilayer volume (Supporting Information). Average center-to-center (d_{cc}) and edge-to-edge (d_{ee}) interfluorophore distances were calculated for a mean vesicle diameter of 150 nm and are listed in Table 1. Using these computed parameters, along with the Figure 1 absorption and emission data, estimates of the orientational parameter, the membrane index of refraction, and fluorescence quantum yield (Supporting Information), the polymersome-dispersed **PZn$_3$** Förster distance (R_{0f}, the center-to-center intermolecular distance at which E_NT between adjacent fluorophores is 50% efficient), is estimated to be ∼6.7 nm. Using this calculated Förster distance, and the computed d_{cc} values, an average energy transfer efficiency (E_f, representing an average quantum yield of excitation energy transfer, Table 1)[63] can be estimated for a given **PZn$_3$** loading, as outlined in the Supporting Information; these energy transfer efficiencies are plotted as a function of loading percentage in Figure S11. Note that fast, sub-50 ps decay of the **3,5-peg-PZn$_3$** excited-state anisotropy signal is significant only at fluorophore:polymer mole ratios

(78) The slight decay at long time delays may indicate that within the experimental timescale, either (i) these energetic barriers are small enough that partial fluorophore rotation within the vesicle matrix occurs or (ii) the vesicles themselves undergo partial rotation; due to the large noise at such long time-delays, rotational correlation times for this loss in polarization cannot be calculated accurately.

(79) Abugo, O. O.; Nair, R.; Lakowicz, J. R. *Anal. Biochem.* **2000**, *279*, 142–150.
(80) Förster, T. *Naturwissenschaften* **1946**, *33*, 166.
(81) Förster, T. *Ann. Phys. Leipzig.* **1948**, *2*, 55.
(82) Assuming a square-well potential for relative molecular orientations, and a locally flat vesicle surface, the critical cone angle, θ_C, calculated from the measured initial (0.39) and final (∼0.1) anisotropies is 51.5° (S = 0.51). A description of this calculation can be found in ref 63, pages 399−401.

Table 1. Effective Molar Concentrations ([**PZn$_3$**]), Estimated Center-to-Center (d_{cc}) and Edge-to-Edge (d_{ee}) Interfluorophore Distances, and Estimated Energy Transfer Efficiencies (E_f) for **PZn$_3$** Fluorophores Dispersed at Various Fluorophore:Polmer Mole Ratios (χ) in **PEO$_{30}$−PBD$_{46}$** (L = 9.6 nm) Polymersomes[a]

loading	χ	[PZn$_3$][b] (mM)	d_{cc}[b] (*nm*)	d_{ee}[b] (*nm*)	E_f[c] (%)
0.1%	0.001	0.4	22.4	19.4	<0.1
0.2%	0.002	0.7	17.8	14.8	0.3
0.4%	0.004	1.5	14.1	11.1	1.1
1%	0.01	3.7	10.4	7.4	6.7
2.5%	0.025	9.2	7.7	4.7	30.3
5%	0.05	18.5	6.1	3.1	63.7
10%	0.1	37.0	4.8	1.8	88.1

[a] For a detailed description of [**PZn$_3$**], d_{cc}, d_{ee}, and E_f calculations, see the Supporting Information. Energy transfer efficiency represents the likelihood that an excited donor fluorophore will pass its excitation energy to a nearby acceptor fluorophore. [b] Determined utilizing a mean vesicle diameter (d) of 150 nm and assuming complete, homogeneous fluorophore dispersion throughout the entire available **PEO$_{30}$−PBD$_{46}$** (L ∼ 9.6 nm) membrane hydrophobic bilayer volume ($V = 1.90 \times 10^{-22}$ M^3). [c] Energy transfer efficiencies were determined from d_{cc} values using an estimated Förster distance (R_{0f}) of 6.7 nm (Supporting Information).

≥2.5% ($\chi \geq 0.025$) (e.g., see the overlaid excited-state anisotropy decay profiles shown in the Supporting Information, Figure S2). Similarly, when the fluorophore:polymer mole ratio exceeds 2.5% in **3,5-peg-PZn$_3$**-based NIR emissive polymersomes, the calculated d_{cc} values are smaller than the determined Förster distance of ∼6.7 nm; energy transfer efficiencies in samples where $\chi > 0.025$ are thus substantial. In samples in which fluorophore:polymer mole ratios are 2.5% and 1% (d_{cc} = 7.7 and 10.4 nm, respectively), adjacent fluorophores are slightly further apart on average than R_{0f} (Table 1), and as a result, the energy-transfer contributions to excited-state depolarization and excited-state quenching dynamics are modest with respect to that evident in more highly loaded samples. Finally, because energy transfer efficiency scales as a factor of d^{-6}, in samples possessing interfluorophore distances even moderately longer than R_{0f} ($\chi < 0.1$), energy migration rapidly becomes inefficient ($E_f < 2\%$) and does not contribute significantly to the excited-state relaxation dynamics (Figure S11).

This analysis reveals an interesting correlation between the onset of reasonably efficient energy transfer (e.g., $E_f > 25\%$) and the onset of significant quenching of the excited-state (e.g., $\tau_{avg} < 450$ ps), which occur in **3,5-peg-PZn$_3$**-based NIR emissive polymersome samples in which the fluorophore:polymer mole ratio is ≥2.5%. Note that integrated fluorescence intensity per vesicle reaches a plateau for the $\chi = 0.025$ nanoscale NIR emissive polyersome samples based on **3,5-peg-PZn$_3$** (Figure S10, Supporting Information). In samples that feature the lowest concentrations of dispersed emitters (e.g., $\chi < 0.01$), note that **3,5-peg-PZn$_3$** fluorophores are >10 nm apart (Table S2, Supporting Information) and excited-state lifetimes are similar in magnitude to those manifested in THF solution ($\tau \sim 1.1$ ns). At high concentrations ($\chi > 0.025$), molecules are close together ($d_{ee} < 5$ nm, Table S2), with ground-state intermolecular interactions evident, as suggested by the broadened ground-state electronic absorption features noted earlier (Figure 1, Table S1). Enhanced populations of **3,5-peg-PZn$_3$** aggregates in nanoscale polymersomes cause: (i) augmented static quenching of the steady-state fluorescence (not reflected in the observed excited-state deactivation rate constants dependences plotted in Figure 3) and (ii) more significant Förster energy migration to trap sites. Reactions A−C summarize this mechanistic model:

$$[\mathbf{PZn_3}]^* \xrightarrow{k_f \text{ (or } k_{ic})} \mathbf{PZn_3} \quad \text{(A)}$$

$$[\mathbf{PZn_3}]^* + \mathbf{PZn_3} \xrightarrow{k_{EnT}} \mathbf{PZn_3} + [\mathbf{PZn_3}]^* \quad \text{(B)}$$

$$[\mathbf{PZn_3}]^* + (\mathbf{PZn_3})_n \xrightarrow{k_{EnT}} \mathbf{PZn_3} + [(\mathbf{PZn_3})_n]^* \xrightarrow{k_{nr}} \mathbf{PZn_3} + (\mathbf{PZn_3})_n \quad \text{(C)}$$

Reaction A represents the decay (fluorescence, internal conversion) of an excited **PZn$_3$** fluorophore ([**PZn$_3$**]*) to its corresponding ground-state (**PZn$_3$**) in the absence of quenching; in nanoscale **PZn$_3$**-based NIR emissive polymersomes where $\chi \leq 0.1\%$, reaction A is the dominant deactivation mechanism and nearly single exponential dynamics are manifest.[83] Reaction B reflects E_NT from [**PZn$_3$**]* to a nearby ground-state **PZn$_3$** acceptor fluorophore, which may impact the excited-state anisotropy, while reaction C denotes E_NT from [**PZn$_3$**]* to a nearby ground-state aggregate complex ((**PZn$_3$**)$_n$). [(**PZn$_3$**)$_n$]* decays quickly ($\tau < 200$ fs) via nonradiative pathways. With respect to reactions B and C, note that the magnitude of the ground-state bleaching signature in the transient absorption experiment is only changed by E_NT events occurring via Reaction C; on the other hand, excited-state anisotropy is only changed by E_NT events occurring via Reaction B, because excited-state decay does not contribute to a loss in excited-state polarization. Because k_{EnT} is proportional to $(d_{cc})^{-6}$, such energy transfer events rapidly become more efficient at fluorophore:polymer mole ratios larger than 1%, as reflected in Figure S11 (Supporting Information) and in the nonlinear dependence of excited-state lifetime as function of **PZn$_3$** concentration (Figure 3). This model is consistent with those proposed for other self-quenching membrane-dispersed fluorophore systems.[53,55,56,59,63,67–69]

C. Excited-State Dynamics of Nanoscale NIR-Emissive Polymersomes Based on 3,5-peg-PZn$_3$ Fluorophores and PEO$_{80}$−PBD$_{125}$ Diblock Copolymers. Figure 5 shows the excited-state decay dynamics of **3,5-peg-PZn$_3$**-based nanoscale NIR emissive polymersomes in which **PZn$_3$** is dispersed at 10 ($\chi = 0.1$) and 1% ($\chi = 0.01$) fluorophore:polymer mole ratios in both **PEO$_{30}$−PBD$_{46}$** (L ∼ 9.6 nm) and **PEO$_{80}$−PBD$_{125}$** (L ∼ 14.8 nm) polymersomes. The decay dynamics measured for supplementary **3,5-peg-PZn$_3$** fluorophore:polymer mole ratios in **PEO$_{80}$−PBD$_{125}$** (L ∼ 14.8 nm) polymersomes are presented in the Supporting Information, Figure S3. The weighted average excited-state lifetime (τ_{avg}) and observed excited-state deactivation rate constant (k_{obs}) values are summarized in Table S2 (Supporting Information). The k_{obs} values are plotted versus χ in Figure 6A and, as observed for similar compositions based on **PEO$_{30}$−PBD$_{46}$** (L ∼ 9.6 nm), increase nonlinearly with increasing fluorophore:polymer mole ratios. Figure 6A also demonstrates that for samples that possess identical fluorophore:polymer mole ratios, k_{obs} for **PZn$_3$** fluorophores dispersed in thinner **PEO$_{30}$−PBD$_{46}$** (L ∼ 9.6 nm) polymersomes are significantly larger than the analogous values recorded for fluorophores dispersed in thicker **PEO$_{80}$−PBD$_{125}$** (L ∼ 14.8 nm) analogs. The Figure 6A data thereby reflect the fact that there is ∼44% more volume available for fluorophore dispersion in **PEO$_{80}$−PBD$_{125}$**-based polymersomes relative to that in

(83) The decay of [**PZn$_3$**]* to **PZn$_3$** via excited triplet-state formation (intersystem crossing) as an intermediate is also implicitly included in Reaction A.

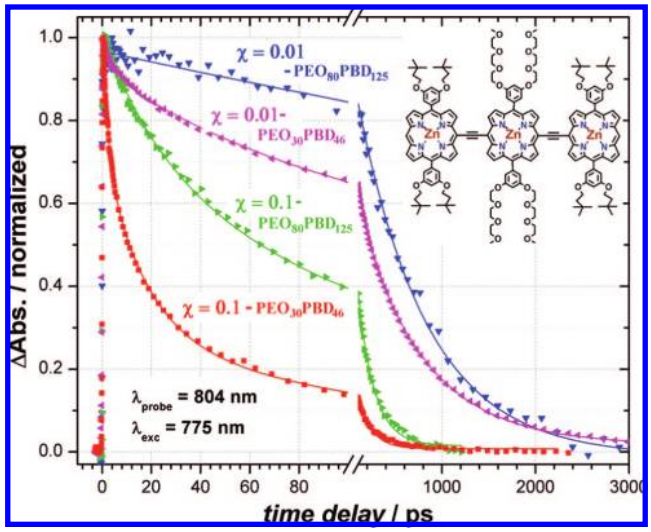

Figure 5. Normalized intensity of the transient bleaching signature centered at 804 nm for **3,5-peg-PZn$_3$** dispersed within **PEO$_{30}$−PBD$_{46}$** ($L \sim 9.6$ nm) and **PEO$_{80}$−PBD$_{125}$** ($L \sim 14.8$ nm) polymersomes at 10 ($\chi = 0.1$) and 1% ($\chi = 0.01$) fluorophore:polymersome molar ratios as a function of time delay. Solid lines represent multiexponential fits of the data. Fitting parameters are tabulated in Table S2 (Supporting Information). Experimental conditions: $\lambda_{exc} = 775$ nm, $\lambda_{probe} = 804$ nm, magic angle polarization, solvent = water, room temperature.

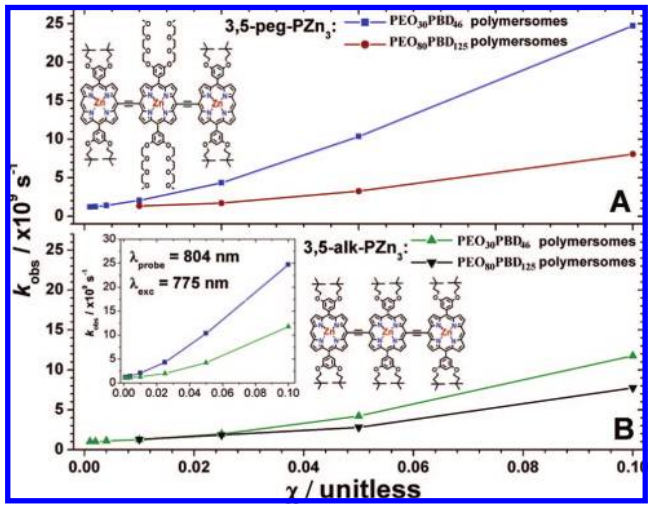

Figure 6. Rate constants for excited-state deactivation (k_{obs} values) for **3,5-peg-PZn$_3$** (A) and **3,5-alk-PZn$_3$** (B) dispersed within **PEO$_{30}$−PBD$_{46}$** ($L \sim 9.6$ nm) and **PEO$_{80}$−PBD$_{125}$** ($L \sim 14.8$ nm) polymersomes as a function of fluorophore-to-polymer molar ratio (χ). The inset in window (B) directly compares k_{obs} vs χ for **3,5-peg-PZn$_3$** and **3,5-alk-PZn$_3$** in **PEO$_{30}$−PBD$_{46}$** polymersomes. Experimental conditions: $\lambda_{exc} = 775$ nm, $\lambda_{probe} = 804$ nm, magic angle polarization, solvent = water, room temperature.

PEO$_{30}$−PBD$_{46}$-based structures; **PEO$_{80}$−PBD$_{125}$**-based NIR emissive polymersomes thus feature smaller effective fluorophore concentrations ([**PZn$_3$**]), larger interfluorophore distances (d_{cc}), fewer aggregate trap sites ([(**PZn$_3$**)$_n$]), and less efficient E_NT to the trap sites (E_f) (Figure 6).

D. Excited-State Dynamics of Nanoscale NIR Emissive Polymersomes Based on 3,5-alk-PZn$_3$ Fluorophores and PEO$_{30}$−PBD$_{46}$ and PEO$_{80}$−PBD$_{125}$ Diblock Copolymers. When the solubilizing side chains pendant to the **PZn$_3$** central porphyrin 10- and 20-aryl moieties are changed from 3,5-bis(9-methoxy-1,4,7-trioxanonyl)phenyl (**3,5-peg-PZn$_3$**) to 3,5-bis(3,3-dimethyl-butoxy)phenyl groups (**3,5-alk-PZn$_3$**), a significant

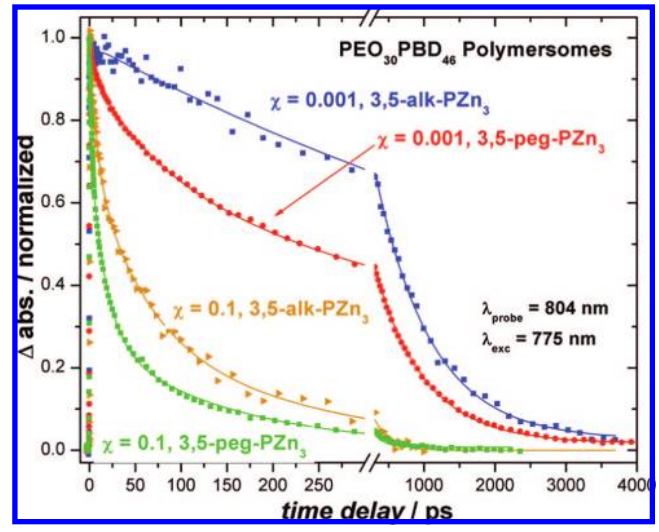

Figure 7. Normalized intensity of the transient bleaching signature centered at 804 nm for **3,5-peg-PZn$_3$** and **3,5-alk-PZn$_3$** dispersed within **PEO$_{30}$−PBD$_{46}$** ($L \sim 9.6$ nm) polymersomes at 10% ($\chi = 0.1$) and 1% ($\chi = 0.001$) fluorophore:polymer molar ratios as a function of time delay. Solid lines represent multiexponential fits of these data. Fitting parameters are tabulated in Table S2 (Supporting Information). Experimental conditions: $\lambda_{exc} = 775$ nm, $\lambda_{probe} = 804$ nm, magic angle polarization, solvent = water, room temperature.

change in the excited-state dynamics observed for **PEO$_{30}$−PBD$_{46}$**-based nanonoscale emissive polymersomes occurs, as demonstrated in Figure 7; the excited-state dynamics interrogated for additional **3,5-alk-PZn$_3$** fluorophore loading levels are plotted in Figure S4 (Supporting Information). At low fluorophore loadings ($\chi \leq 0.004$), the decay dynamics are dominated by single exponential functions in which the associated amplitudes exceed 90%, whereas at high ($\chi \geq 0.025$) fluorophore loadings, several exponential terms are required to accurately model the decay dynamics, reflecting the importance of additional pathways for excited-state decay for these systems. Note, however, that the associated amplitude of the primary exponential component is nearly 90% even for the moderately loaded $\chi = 0.01$ (1% fluorophore:polymer mole ratio) nanoscale NIR emissive polymersome composition based on **3,5-alk-PZn$_3$**; analogous **3,5-peg-PZn$_3$/PEO$_{30}$−PBD$_{46}$** emissive polymersomes featuring a 1% fluorophore:polymer mole ratio ($\chi = 0.01$) exhibit clear multiexponential dynamics, with an associated amplitude for the primary exponential decay component of only 65%. These data thus show that for identical fluorophore loading levels, membrane-dispersed **3,5-peg-PZn$_3$** excited-states decay faster than the analogous states of membrane-dispersed **3,5-alk-PZn$_3$**. This is further exemplified in the Figure 6B inset, which plots k_{obs} as a function of χ for these two **PZn$_3$** fluorophores dispersed in **PEO$_{30}$−PBD$_{46}$** ($L \sim 9.6$ nm) polymersomes, and shows that the k_{obs} values for polymersomes based on **3,5-peg-PZn$_3$** increase more rapidly as a function of χ than those determined for analogous vesicles that disperse **3,5-alk-PZn$_3$**. This is in agreement with fluorescence data (Figure S10, Supporting Information), which shows that for a given fluorophore loading, polymersomes containing **3,5-alk-PZn$_3$** are more emissive than those dispersing **3,5-peg-PZn$_3$**.

Assuming that Förster distances (and hence, energy transfer efficiencies) are similar for nanoscale polymersomes that disperse **3,5-alk-PZn$_3$** and **3,5-peg-PZn$_3$** fluorophores, the explanation for this result must lie in an increased concentration of trap sites in nanoscale **3,5-peg-PZn$_3$/PEO$_{30}$−PBD$_{46}$** poly-

mersomes relative to analogous **3,5-alk-PZn$_3$/PEO$_{30}$−PBD$_{46}$** compositions. This conclusion is supported by transient anisotropy experiments: while excited-state lifetimes in membrane-dispersed **3,5-peg-PZn$_3$** fluorophores are generally shorter than in membrane-dispersed **3,5-alk-PZn$_3$** fluorophores, the transient anisotropy decay follows the reverse trend; note that the transient anisotropy of **3,5-alk-PZn$_3$** dispersed at 10% fluorophore: polymer mole ratio in **PEO$_{30}$−PBD$_{46}$** ($L \sim 9.6$ nm) polymersomes ($\tau_{R,avg} \approx 3.3$ ps) actually decays faster than that for analogous **3,5-peg-PZn$_3$**-based emissive vesicles ($\tau_{R,avg} \approx 14.3$ ps) (Figure S5). As the transient anisotropy decay reflects only hopping events to nonaggregated chromophores (i.e., Reaction B, above), not to trap-sites (Reaction C), which do not contribute to a loss of polarization, these data indicate that for n energy transfer events, the probability of transfer to a dark trap site is higher for NIR-emissive polymersomes dispersing **3,5-peg-PZn$_3$** than for those that disperse **3,5-alk-PZn$_3$**. Conversely, the probability of transfer to a nonaggregated **PZn$_3$** fluorophore is lower in nanoscale **3,5-peg-PZn$_3$/PEO$_{30}$−PBD$_{46}$** polymersomes than **3,5-alk-PZn/PEO$_{30}$−PBD$_{46}$** based vesicles, as demonstrated by the transient anisotropy and excited-state dynamical data.

There are two possible explanations for the increased likelihood of energy transfer to trap sites in polymersomes loaded with **3,5-peg-PZn$_3$** versus those loaded with **3,5-alk-PZn$_3$**: (i) the equilibrium constant for **(3,5-peg-PZn$_3$)$_n$** aggregate formation is greater than that for **(3,5-alk-PZn$_3$)$_n$** aggregates at identical **PZn$_3$**:polymer ratios in nanoscale polymersomes, or (ii) the effective fluorophore molar concentration in these nanoscale bilayered vesicles for identical **PZn$_3$** polymer compositions is greater **for 3,5-peg-PZn$_3$** than for **3,5-alk-PZn$_3$**. This latter explanation requires that the effective distribution volumes for **3,5-peg-PZn$_3$** and **3,5-alk-PZn$_3$** in similar sized nanoscale polymersomes are not identical.

To test whether polymersome distribution volumes for **3,5-peg-PZn$_3$** and **3,5-alk-PZn$_3$** differ, the excited-state dynamics of **3,5-alk-PZn$_3$** dispersed in **PEO$_{80}$−PBD$_{125}$** ($L \sim 14.8$ nm) polymersomes at various fluorophore loading percentages were interrogated (Figure S6, Supporting Information). Fluorophore excited-state lifetimes (τ_{avg}) and corresponding observed excited-state deactivation rate constants (k_{obs}) are tabulated in Table S2; these k_{obs} values are plotted as a function of **3,5-alk-PZn$_3$** loading in Figure 6B along with analogous data obtained for **PEO$_{30}$−PBD$_{46}$** ($L \sim 9.6$ nm) polymersomes for comparison. These data show that changing the constituent polymersome polymer from **PEO$_{30}$−PBD$_{46}$** ($L \sim 9.6$ nm) to **PEO$_{80}$−PBD$_{125}$** ($L \sim 14.8$ nm) results in a large reduction of k_{obs} for equivalent **3,5-peg-PZn$_3$** loading percentages (Figure 6A); in contrast, when the dispersed fluorophore is **3,5-alk-PZn$_3$** (Figure 6B), only a relatively small reduction of k_{obs} for equivalent loading percentages occurs. Increasing vesicle thickness thus reduces the magnitude of the observed excited-state deactivation rate constant in polymersomes dispersing **3,5-peg-PZn$_3$** to a much greater extent than those that disperse **3,5-alk-PZn$_3$**. These data thus indicate that **3,5-peg-PZn$_3$** and **3,5-alk-PZn$_3$** fluorophores do not possess identical polymersomal distribution volumes.

If a given **PZn$_3$** fluorophore occupies the entire available hydrophobic bilayer volume when dispersed within both **PEO$_{30}$−PBD$_{46}$** ($L \sim 9.6$ nm) and **PEO$_{80}$−PBD$_{125}$** ($L \sim 14.8$ nm) polymersomes, then converting fluorophore:polymer mole ratios (χ) into absolute fluorophore molar concentrations, **[PZn$_3$]** (i.e., normalizing χ for the respective available **PEO$_{30}$−PBD$_{46}$** and **PEO$_{80}$−PBD$_{125}$** fluorophore dispersion volumes) should result in a similar quantitative dependency of k_{obs} on **[PZn$_3$]** regardless of whether **PZn$_3$** is dispersed in polymersomes comprised of **PEO$_{30}$−PBD$_{46}$** or **PEO$_{80}$−PBD$_{125}$**; on the other hand, if the fluorophore is localized in a volume element smaller than the entire hydrophobic bilayer, then the excited-state dynamical data obtained for **PEO$_{30}$-PBD$_{46}$-** ($L \sim 9.6$ nm) and **PEO$_{80}$−PBD$_{125}$**-based ($L \sim 14.8$ nm) emissive polymersome systems will display disparate dependences of k_{obs} on **[PZn$_3$]** as the computed molar concentrations will not scale as described above. Figure 8 demonstrates such a normalization of the Figure 6 $k_{obs}(\chi)$ data for both membrane-dispersed **3,5-peg-PZn$_3$** (Figure 8A) and **3,5-alk-PZn$_3$** (Figure 8B). Figure 8B shows that **PEO$_{30}$−PBD$_{46}$**-dispersed and **PEO$_{80}$−PBD$_{125}$**-dispersed **3,5-alk-PZn$_3$** fluorophores exhibit a similar quantitative dependency of k_{obs} on **[PZn$_3$]**, indicating that **3,5-alk-PZn$_3$** is dispersed throughout the entire available hydrophobic bilayer volume; conversely, Figure 8A shows that **PEO$_{30}$−PBD$_{46}$**-dispersed and **PEO$_{80}$−PBD$_{125}$**-dispersed **3,5-peg-PZn$_3$** fluorophores do not exhibit a similar quantitative dependency of k_{obs} on **[PZn$_3$]**. These data indicate that **3,5-peg-PZn$_3$** must be localized in a volume element smaller than the entire hydrophobic polymersome core. Thus, absolute (local) fluorophore concentrations are higher for polymersomes loaded with **3,5-peg-PZn$_3$** than for those loaded with **3,5-alk-PZn$_3$** at identical fluorophore: polymer molar ratios, leading to a larger concentration of dark trap sites per nanoscale vesicle, and a diminished integrated emission intensity relative to analogous polymersomes that disperse **3,5-alk-PZn$_3$**.

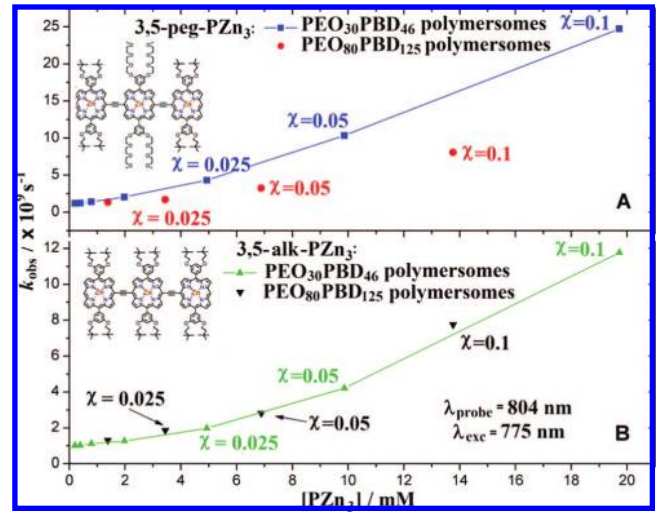

Figure 8. Observed rate constants for excited-state deactivation (k_{obs} values) for polymersome-dispersed **3,5-peg-PZn$_3$** (A) and **3,5-alk-PZn$_3$** (B) emitters plotted as a function of absolute fluorophore molar concentration (**[PZn$_3$]**), calculated assuming uniform dissolution throughout the entire bilayer volume (Supporting Information) for a vesicle diameter of 150 nm.

A model that accounts for the disparate polymersomal distribution volumes for **3,5-peg-PZn$_3$** and **3,5-alk-PZn$_3$** should, after adjusting for the actual occupied fractional volume, provide a similar quantitative dependency of k_{obs} on **[3,5-peg-PZn$_3$]** for both **PEO$_{30}$−PBD$_{46}$-** and **PEO$_{80}$−PBD$_{125}$**-based vesicles, as was observed for the polymersome-dispersed **3,5-alk-PZn$_3$** dynamical data highlighted in Figure 8B. One simple model that accounts for a reduced **3,5-peg-PZn$_3$** distribution volume is depicted in Figure 9.[48] Due to its relative hydrophilicity, **3,5-peg-PZn$_3$** should exhibit augmented solubility in the peripheral regions of the vesicle bilayer (α regions, Figure 9) where there would be a higher concentration of diffused water molecules,

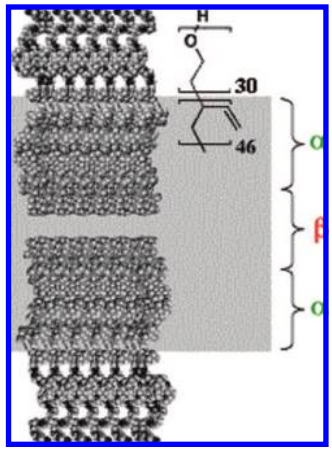

Figure 9. Two subregions of the hydrophobic polymersome bilayer, relatively polar α - green (peripheral) vs relatively nonpolar β - red (interior).

relative to **3,5-alk-PZn$_3$**. Conversely, more hydrophobic **3,5-alk-PZn$_3$** fluorophores should manifest no such propensity to localize in the peripheral α regions, and should disperse throughout a near maximal bilayer volume (α and β regions, Figure 9). Restricting **3,5-peg-PZn$_3$** fluorophores only to the peripheral α regions (α region thicknesses ≈ 3.7 nm) leads to the convergence of the k_{obs} data recorded in **PEO$_{30}$−PBD$_{46}$** and **PEO$_{80}$−PBD$_{125}$**-based polymersomes when normalized to [**PZn$_3$**], as was observed for polymersome-dispersed **3,5-alk-PZn$_3$** in which the entire available membrane volume was utilized to compute [**PZn$_3$**] (data not shown).

E. Excited-State Dynamics of Nanoscale NIR-Emissive Polymersomes Based on 2,6-alk-PZn$_3$ Fluorophores and PEO$_{30}$−PBD$_{46}$ Diblock Copolymers. As an additional example of how fluorophore chemical structure affects nanoscale emissive polymerosome excited-state dynamics, vesicles that disperse **2,6-alk-PZn$_3$** fluorophores were investigated. The ground- and excited-state electronic structures of **2,6-alk-PZn$_3$** and **3,5-alk-PZn$_3$** are virtually identical,[48] as these emitters differ only with respect to the positions of attachment (3,5- vs 2,6-) of the solubilizing 3,3-dimethylbutyloxy ether groups to the ancillary 10- and 20- phenyl rings of the component **PZn** building blocks of these **PZn$_3$** fluorophores (Chart 1). Note, however, that changing the substitution pattern on the *meso* phenyl rings from 3,5 to 2,6 significantly alters the chromophores' gross structure from a biconcave wedge to a cylinder. As a result of this structural effect, **2,6-alk-PZn$_3$** is solubilized less effectively by the constituent polymer strands, thereby driving enhanced aggregate formation, as indicated by the steady-state optical spectra (Figure 1).

The excited-state dynamics of **2,6-alk-PZn$_3$** dispersed at 0.1 and 10% fluorophore:polymer molar ratios in **PEO$_{30}$−PBD$_{46}$** polymersomes are provided in the Supporting Information, Figure S13. These data sets exhibited substantial noise levels due to their very weak transient absorption signals, even at relatively high (∼5 mJ/cm^2) pump fluences; ΔAbs values in these experiments were only on the order of 2−3 mOD. Transient anisotropy experiments (Figures S7 and S8, Supporting Information) indicate that the excited-state anisotropy of **2,6-alk-PZn$_3$/PEO$_{30}$−PBD$_{46}$** polymersomes essentially remains unchanged (r(t) ∼ 0.36−0.37) as a function of time delay even at a 10% fluorophore:polymer loading ratio. The transient dynamical data highlighted in Figures S7, S8 and S13 (Supporting Information), in addition to the steady-state absorption and emission data discussed earlier, underscore several conclusions regarding the photophysics of membrane-dispersed **2,6-alk-PZn$_3$**: (i) **2,6-alk-PZn$_3$** efficiently forms trap aggregates, even at low loadings, potentially due to its inability to easily intercalate between polymer strands; (ii) these trap aggregates have very short excited-state lifetimes (τ < 200 fs), giving rise to weak initial transient absorption signals that derive from large amplitude static quenching of the **2,6-alk-PZn$_3$** excited-state at all polymersome loading levels; (iii) due to a substantial concentration of (**2,6-alk-PZn$_3$**)$_n$ trap aggregates, excitation energy migration from electronically excited nonaggregated chromophores results in high probability energy transfer to quenching sites (Reaction C, above). Because energy migration to quenching sites does not contribute to loss of excited-state anisotropy, excited-state anisotropy remains relatively constant as a function of time delay, even at 10% fluorophore loading.

F. Excited-State Dynamics of Nanoscale NIR-Emissive Polymersomes Based on 3,5-peg-PZn$_5$ Fluorophores in PEO$_{30}$−PBD$_{46}$ Diblock Copolymers. A full account of the excited-state dynamics of pentameric **3,5-peg-PZn$_5$** fluorophores dispersed in **PEO$_{30}$−PBD$_{46}$** polymersomes is provided in the Supporting Information.

Conclusions

While fluorescent, organic-based nanoparticles have garnered increased attention due to the potential to engineer extensive structural diversity, biocompatibility, and properties important for optoelectronics and targeted probes, there has been a paucity of studies that systematically explored factors that influence the emissive output of such structures. This report describes the first ultrafast time-domain pump−probe spectroscopic investigation of a fluorescent organic-based nanoparticle system.

Excited-state dynamical studies of NIR-emissive polymersomes incorporating a series of ethynyl-bridged oligo(porphinato)zinc(II)-based (**PZn$_n$**) supermolecular fluorophores: (1) Demonstrate the utility of the time-dependent excited-state anisotropy experiment, which evinces that the dominant mechanism for fluorescence quenching at high (>2.5 mol%) fluorophore:polymer mole ratios is energy migration to trap sites (ground-state aggregates). Such fluorescence quenching dynamics, governed by donor-donor energy migration processes, have been complicated by rotational diffusion in other studies of membrane-dispersed fluorophores;[52,55,56,60,62,84] partially mobile fluorophores that drive polarization loss are absent in a polymersome environment, as the component diblock copolymers of these vesicles enforce a large barrier to **PZn$_n$** rotation; (2) underscore that the per-fluorophore fluorescence quantum yield at a given **PZn$_n$**:polymer mole ratio can be modulated through variation of the polymersome hydrophobic bilayer thickness. Augmenting the hydrophobic core thickness increases the total available volume for fluorophore dispersion, and hence diminishes the concentration of trap aggregates; and (3) highlight that the magnitude of the vesicular emissive output depends upon fluorophore structure. For example, **3,5-peg-PZn$_3$** and **3,5-alk-PZn$_3$** differ only in the nature of their pendant porphyrinic side chains and thus have identical photophysical properties in solution; in contrast, transient absorption and anisotropy decay data acquired for **3,5-peg-PZn$_3$**- and **3,5-alk-PZn$_3$**-loaded nanoscale polymersomes show that these two fluorophores manifest disparate dispersion volumes that correlate with the

(84) Lakowicz, J. R.; Prendergast, F. G.; Hogen, D. *Biochemistry* **1979**, *18*, 520–527.

hydrophilicity of their respective solubilizing groups, which thereby modulate time-dependent nanoparticle emission intensity.

In summary, this study interrogates key relationships between fluorophore structure, nanoparticle composition, and observed excited-state dynamics in nanoscale NIR-emissive polymersomes, and demonstrates that ultrafast excited-state absorption and anisotropy dynamics can be used in tandem to: (i) correlate fluorophore structure with its gross spatial arrangement within specific nanodomains of a nanoparticle and (ii) reveal how compartmentalization of fluorophores within reduced effective dispersion volumes impacts bulk photophysical properties. As these factors play key roles in determining the energy transfer dynamics between dispersed fluorophores, this work underscores that strategies that modulate fluorophore and polymer structure to minimize emitter orientational heterogeneity and optimize dispersion volume in bilayered nanoscale vesicular environments will further enhance the emissive properties of these sensitive nanoscale imaging agents.[43]

Acknowledgment. This work was supported by a grant from the Department of Energy DE-FGO2-02ER15299. T.V.D. acknowledges a Carolyn Hoff Lynch Graduate Fellowship, and P.P.G. thanks the NIH Medical Scientist Training Program and the Whitaker Foundation for support. We are grateful also to the National Institutes of Health (R01CA115229), and the MRSEC (DMR0079909) and NSEC (DMR04-25780) programs of the National Science Foundation, for infrastructural support.

Supporting Information Available: Dynamical data, steady-state absorption and emission data, computational data and methods, supplemental figures and tables, description of transient dynamics of **3,5-peg-PZn$_5$** fluorophores dispersed in **PEO$_{30}$−PBD$_{46}$** diblock copolymers. This material is available free of charge via the Internet at http://pubs.acs.org.

JA711497W